Korean J. Chem. Eng., 35(12), 2327-2335 (2018)
DOI: 10.1007/s11814-018-0134-5

pISSN: 0256-1115
eISSN: 1975-7220

Modeling, simulation and structural analysis of a fluid catalytic cracking (FCC) process

Sungho Kim*, Jaejung Urm*, Dae Shik Kim*, Kihong Lee, and Jong Min Lee*,†**

*School of Chemical and Biological Engineering, Institute of Chemical Processes, Seoul National University, 1 Gwanak-ro, Gwanak-gu, Seoul 08826, Korea
**Hyundai Oilbank Co., 182 Pyeongsin 2-ro, Daesan-eup, Seosan-si, Chungcheongnam-do 31902, Korea
(*Received 17 May 2018 • accepted 26 July 2018*)

Abstract−Fluid catalytic cracking (FCC) is an important chemical process that is widely used to produce valuable petrochemical products by cracking heavier components. However, many difficulties exist in modeling the FCC process due to its complexity. In this study, a dynamic process model of a FCC process is suggested and its structural observability is analyzed. In the process modeling, yield function for the kinetic model of the riser reactor was applied to explain the product distribution. Hydrodynamics, mass balance and energy balance equations of the riser reactor and the regenerator were used to complete the modeling. The process model was tested in steady-state simulation and dynamic simulation, which gives dynamic responses to the change of process variables. The result was compared with the measured data from operating plaint. In the structural analysis, the system was analyzed using the process model and the process design to identify the structural observability of the system. The reactor and regenerator unit in the system were divided into six nodes based on their functions and modeling relationship equations were built based on nodes and edges of the directed graph of the system. Output-set assignment algorithm was demonstrated on the occurrence matrix to find observable nodes and variables. Optimal locations for minimal addition of measurements could be found by completing the whole output-set assignment algorithm of the system. The result of this study can help predict the state more accurately and improve observability of a complex chemical process with minimal cost.

Keywords: Fluid Catalytic Cracking, Yield Function, Process Modeling, Structural Observability, Occurrence Matrix

INTRODUCTION

Fluid catalytic cracking (FCC) is one of the most important refinery processes. It is used for cracking high molecular weight hydrocarbon feedstocks to smaller molecules which boil at relatively lower temperatures. The common industrial FCC process consists of a cracking reactor followed by a catalyst regenerator and fractionation units that separate the reactor effluent into the final products. Although the FCC process has been long studied, modeling the FCC process is very difficult because the number of chemical species in the reaction system is very large and each species can affect various cracking reactions [1]. There is also a large amount of uncertainty in the kinetics of the reactions. Thus, modeling every cracking reaction in the system is impractical. Instead, to model such complex mixtures, a structure-oriented lumping (SOL) approach which considers the molecular structure has been suggested [2]. However, industrial application of SOL is difficult since the analysis of petroleum fractions is very limited in practice.

In the discrete lumping approach [3], the mixture is assumed to be composed of pure pseudo-components that are characterized by physical properties such as normal boiling point (NBP). Most of the existing studies for discrete lumping use a small number of pseudo-components to reduce the number of unknown parameters. In early studies [4,5] the reaction was represented by using three lump groups, feed, gasoline and light gases. Coke and light gases were also considered as separate lump groups [6-8]. Later studies also included diesel as another lump [9-11]. Up to ten lump models are reported in the literature [12-14]. It was also assumed that each pseudo-component gives two other pseudo-components in one single reaction step [3]. They estimated the kinetic parameters using a probability based empirical approach that considers every unit reaction.

Meanwhile, knowing the internal state of a complicated system is important for process modeling, control and optimization. However, measuring all the state variables of an operating FCC process is usually impossible or impractical. Instead, estimation of the state variables based on a finite set of measurements is widely performed in the industry. For that purpose, system observability which characterizes whether a given set of measurements is sufficient to estimate any state of the system is analyzed. Structural observability is a fundamental property that provides a necessary condition for system observability, and often it may also be sufficient for many complex chemical process [15,16]. Structural observability analysis can be done using graph-theoretic techniques and modeling relationship. Unknown parameters and states can be estimated by augmenting the state variables to include the unknown parameters, and it is necessary to check the observability of the augmented system. Structural observability analysis via graph theory offers a visual means to pinpoint measurements needed to estimate states or to detect which cannot be estimated with given system and measurements [17]. In addition to analyzing the observability for a given set of measurements, it would be also useful to determine a minimal set of

†To whom correspondence should be addressed.
E-mail: jongmin@snu.ac.kr

measurements which make the process systematically observable, especially for large-scale complex systems.

In this study, a dynamic model of a FCC plant including a reactor and a regenerator is first presented. To describe kinetics of cracking reactions, a yield function was constructed to calculate the product distribution from a specific pseudo-component. Steady-state process simulation and dynamic simulation that find responses to change of several process variables were performed. Since industrial FCC processes lack the measurements for optimization, structural analysis of the FCC process was performed to find observability of the process. A directed graph was drawn to construct modeling relationships of the system and an occurrence matrix. Output-set assignment algorithm was then performed on the occurrence matrix by solving the matrix sequentially. Optimal locations for additional measurements were suggested by completing the whole output-set assignment algorithm of the system under the assumption of additional measurement. The result of this study can help predict the state more accurately and improve observability of a complex chemical process such as the FCC process.

MODELING OF THE FCC PROCESS

The scope of FCC plant modeled in this study includes the riser reactor and the catalyst regenerator. These units are modeled individually and connected for investigating the dynamic response.

1. Modeling of the Riser Reactor

1-1. Material Balances

The residue feed is mixed with hot catalyst and steam at the bottom of the reactor. The mixed feed is spread in the feed inlet zone and vaporized by heat from hot catalyst and steam. This zone is considered as an imaginary vessel with a very small volume. Therefore, this volume can be modeled as a separate unit in which the feed is mixed uniformly but the cracking reactions do not occur. Under these assumptions, a steady-state energy balance for the inlet zone is:

$$\int_{T_{regen}}^{T_{mixzone}} \dot{M}_{cat} \times C_{p,\,cat}\,dT = \sum_{i=1}^{N} \int_{T_{HVGO}}^{T_{B,\,i}} \dot{M}_i \times C_{p,\,liquid,\,i}\,dT + \sum_{i=1}^{N} \Delta H_{vap,\,i} + \sum_{i=1}^{N} \int_{T_{B,\,i}}^{T_{jmixzone}} \dot{M}_i \times C_{p,\,gas,\,i}\,dT + \int_{T_{steam}}^{T_{mixzone}} \dot{M}_{steam} \times C_{p,\,steam}\,dT \quad (1)$$

This equation is the energy balance between catalyst particle, liquid feed and steam. Hydrocarbon feeds are vaporized by the heat supplied by catalyst and steam. The gas velocity of the mixture is calculated from the ideal gas law:

$$v_g = \frac{\dot{M}_{HVGO} \times R \times T_{mixzone}}{MW \times P \times A_{riser}} \quad (2)$$

The gas velocity calculated from Eq. (2) is considered to be kept constant in the riser reactor.

In the reaction zone after the feed inlet zone vaporized hydrocarbon feeds and catalyst particles flow along the reactor, and the cracking reactions occur. The reactor is modeled as a single-phase plug-flow reactor and only axial position of the flow is considered. At the reactor exit, deactivated catalyst is separated from the reactor effluent and sent to the regenerator.

The pressure drop in the riser reactor is calculated by [18,19]

$$\frac{\partial P}{\partial z} = -((1-\varepsilon)\rho_{cat} + \varepsilon\rho_g)g - \frac{\partial}{\partial z}((1-\varepsilon)\rho_{cat} v_{cat}^2 + \varepsilon\rho_g v_g^2) \quad (3)$$

$$\varepsilon = 1 - \frac{\dot{M}_{cat}}{v_{cat}\rho_{cat}A_{riser}} \quad (4)$$

where ε is the void fraction of the catalyst volume in the gas rising along the reactor. The pressure drop across the riser reactor is mainly affected by gas velocity changes through temperature decrease during the reaction [20].

The catalyst velocity is calculated from

$$\frac{\partial v_{cat}}{\partial z} = C_D \frac{3\rho_g \times (v_g - v_{cat})^2}{4\, d_{cat}\rho_{cat} v_{cat}} + \frac{(\rho_g - \rho_{cat})}{\rho_{cat} v_{cat}} g \quad (5)$$

C_D is the drag coefficient of catalyst particle, and d_{cat} is the diameter of the catalyst particles. The catalyst velocity is also affected by the gravitational forces. Mixture of gas and catalyst is considered to move simultaneously, and the velocity of gas and catalyst is assumed to be the same to reduce the computing time as the size of the catalyst particles are small.

Rate constants of the cracking reactions in this study are defined as a function of a normal boiling point.

$$k_i = A_i e^{(-E_{A,\,i}/RT)} \quad (6)$$

$$E_{A,\,i} = E_1 - (E_2 \times NBP_i) \quad (7)$$

$$A_i = \beta \times NBP_i^{\mu} \quad (8)$$

Since the reactants with higher boiling points have higher cracking rate constants [21,22], the rate constant is expressed as a power law.

To explain the product distribution from cracking reactions, the yield function p(i, j) is built to calculate the products distribution from cracking of a specific pseudo-component; p(i, j) denotes the yield of each elementary reaction where a component i is converted to j. Each component can be converted to any of the lighter components. The product distribution of a cracking reaction can be represented by the normal boiling point of each lump group [14]. The product distribution of a similar petroleum feed group [18,21,23] was also used to build the yield function. P_j^T is the normalization factor of yield functions. In this study, residue feed was cracked into off-gas, liquefied petroleum gas (LPG), whole crack naphtha (WCN), light cycle oil (LCO) and cycle oil (CLO). NBP distribution data was collected from [23].

$$p(i, j) = \frac{1}{P_j^T}\sqrt{\frac{\lambda_p \times NPB_j}{2\pi \times NBP_i^3}}\, e^{\frac{-\lambda_p \times NBP_i}{(\mu_p \times NBP_j)^2 NBP_i}(NBP_i - (\mu_p \times NBP_j)^2)} \quad (9)$$

$$P_j^T = \sum_{i}^{j-1} \sqrt{\frac{\lambda_p \times NPB_i}{2\pi \times NBP_i^3}}\, e^{\frac{-\lambda_p \times NBP_i}{(\mu_p \times NBP_j)^2 NBP_i}(NBP_i - (\mu_p \times NBP_j)^2)} \quad (10)$$

The steady-state mass balance equation including the reaction of each pseudo-components is:

$$\frac{\partial \dot{M}_i}{\partial z} = -k_i \times \frac{\dot{M}_i}{v_g} \times (1-\varepsilon) \times \rho_{cat} \times \Phi \quad (11)$$

$$+\sum_{n>i}^{N} p(i, n)\times(1-\varphi)\times k_n\times\frac{\dot{M}_i}{v_g}\times(1-\varepsilon)\times\rho_{cat}\times\Phi$$

The first term in the right hand side means the cracking reaction of the i^{th} component to form smaller components. The second term is the formation of the i^{th} component from cracking of heavier components.

There is some proportion of hydrocarbons which are deposited on the surface of solid catalyst due to coking. Since this phenomenon hinders cracking reactions by deactivating the catalyst, the amount of generated coke should be predicted. For this reason, coking parameter (φ) was introduced in the mass balance equation.

1-2. Energy Balances

The steady-state energy balance for axial position z is given by

$$\frac{\partial(\dot{M}\times C_{p,avg}\times T+\dot{M}_{cat}\times C_{p,cat}\times T)}{\partial z} = \sum_{i=1}^{N}\Delta H_i\times k_i\times\frac{\dot{M}_i}{v_g}\times(1-\varepsilon)\times\rho_{cat}\times\Phi \quad (12)$$

The heat supplied by the catalyst is used for the endothermic cracking reactions.

The heat of cracking of the i^{th} component is calculated from [3],

$$\Delta H_i = H_{c,coke}\times\varphi+\sum_{j=1}^{i} p(i, j)\times(1-\varphi)\times H_{c,j}-H_{c,i} \quad (13)$$

where $H_{c,coke}$ is the heat of combustion of coke and $H_{c,i}$ is the heat of combustion of the i^{th} component.

2. Modeling of the Regenerator

In the regenerator, the coke deposited on catalyst surface is removed by burning in air to increase the catalyst activity. The air is fed to the bottom of the regenerator and reacts with the coke and other pollutants on the catalyst. Since combustion reactions are highly exothermic, the temperature of regenerated catalyst is very high. After the regeneration, the catalyst is transferred to the riser reactor and mixed with the feed. It provides energy for vaporization of the feed and the endothermic reactions in the riser reactor.

The regenerator is assumed to consist of two physical phases: solid dense bed and vapor dilute phase. At the boundary between two phases, the catalyst particle freely shifts from each phase [24]. These phases are modeled separately.

2-1. The Dense Bed Phase

The dense bed is the lower part of the regenerator unit with higher concentration of catalyst particles. Coke and other pollutants on the catalyst react with oxygen in the air. To make our model simpler, the dense bed was assumed to be a single-phase and well-mixed reactor.

We assumed that the catalyst holdup is kept constant by controlling the flow of the regenerated catalyst circulation flow. The reaction mechanism is not fully defined due to the influence of catalyst, uncertainty of reaction parameters and complex hydrodynamics. Regeneration reactions and rate expressions were adapted from [13,26]. In this model, carbon molecule is burned to generate CO_2 via direct conversion or intermediate reaction which generates CO and CO_2. The reaction rates are given by

$$\text{(Reaction I)}\ r_{C,CO}=k_{C,CO}\left(\frac{M_{cat}}{V_{densebed}}\times\frac{Y_{coke}^{regen}}{MW_{coke}}\right)^{a_1}\times(P_{O_2})^{a_2} \quad (14)$$

$$\text{(Reaction II)}\ r_{C,CO_2}=k_{C,CO_2}\left(\frac{M_{cat}}{V_{densebed}}\times\frac{Y_{coke}^{regen}}{MW_{coke}}\right)^{a_3}\times(P_{O_2})^{a_4} \quad (15)$$

$$\text{(Reaction III)}\ r_{CO,CO_2,c}=k_{CO,CO_2,c}\times\frac{M_{cat}}{V_{densebed}}\times(P_{CO})^{a_5}\times(P_{O_2})^{a_6} \quad (16)$$

$$\text{(Reaction IV)}\ r_{CO,CO_2,h}=k_{CO,CO_2,h}\times(P_{CO})^{a_7}\times(P_{O_2})^{a_8} \quad (17)$$

Unlike the riser reactor, the dynamics of the dense bed phase are significant due to the large catalyst holdup of catalysts and its effect on the energy balances. The approximate residence time of the catalyst in the dense bed is about 5-10 min, which is much longer than 5-10 seconds in the riser reactor. The mass balance for the coke is expressed by the coke weight fraction on catalyst, which is given by

$$\frac{M_{cat}}{MW_{coke}}\frac{d}{dt}(Y_{coke}^{regen})=\dot{M}_{cat}\frac{Y_{coke}^{riser}}{MW_{coke}} -\dot{M}_{cat}\frac{Y_{coke}^{regen}}{MW_{coke}}-(r_{C,CO}+r_{C,CO_2})V_{densebed} \quad (18)$$

where $(r_{C,CO}+r_{C,CO_2})$ is the combustion rate of coke.

The gaseous species resides in the dense bed about five seconds. Therefore, it is assumed that pseudo-steady state for the gaseous phase in the regenerator. The mass balance for CO in the dense phase from the four reactions is

$$-\dot{M}_{CO,DensetoDilute}+r_{CO}V_{densebed}=0 \quad (19)$$

$$r_{CO}=k_{C,CO}\left(\frac{M_{cat}}{V_{densebed}}\times\frac{Y_{coke}^{regen}}{MW_{coke}}\right)^{a_1}\times(P_{O_2})^{a_2}-k_{CO,CO_2,c} \times\frac{M_{cat}}{V_{densebed}}\times(P_{CO})^{a_5}\times(P_{O_2})^{a_6}-k_{CO,CO_2h}\times(P_{CO})^{a_7}\times(P_{O_2})^{a_8} \quad (20)$$

In the same manner, the material balance of CO_2 is given by

$$-\dot{M}_{CO_2,DensetoDilute}+r_{CO_2}V_{densebed}=0 \quad (21)$$

$$r_{CO_2}=k_{C,CO_2}\left(\frac{M_{cat}}{V_{densebed}}\times\frac{Y_{coke}^{regen}}{MW_{coke}}\right)^{a_1}\times(P_{O_2})^{a_2}-k_{CO,CO_2,c} \times\frac{M_{cat}}{V_{densebed}}\times(P_{CO})^{a_5}\times(P_{O_2})^{a_6}-k_{CO,CO_2h}\times(P_{CO})^{a_7}\times(P_{O_2})^{a_8} \quad (22)$$

H_2 generated during the reaction is converted to H_2O instantly and leaves the dense bed phase. Flow rates of the H_2O and O_2 are given by

$$\dot{M}_{H_2O,DensetoDilute}=\dot{M}_{cat}Y_{coke}^{riser}\frac{Y_{H_2}^{riser}}{MW_{H_2}} \quad (23)$$

$$\dot{M}_{O_2,in}-\dot{M}_{H_2O,DensetoDilute}-\dot{M}_{cat}Y_{coke}^{riser}\frac{Y_{H_2}^{riser}}{MW_{H_2}}+r_{O_2}V_{Densebed}=0 \quad (24)$$

$$r_{O_2}=-k_{C,CO}\left(\frac{M_{cat}}{V_{densebed}}\times\frac{Y_{coke}^{regen}}{MW_{coke}}\right)^{a_1}\times(P_{O_2})^{a_2} -k_{C,CO_2}\left(\frac{M_{cat}}{V_{densebed}}\times\frac{Y_{coke}^{regen}}{MW_{coke}}\right)^{a_3}\times(P_{O_2})^{a_4}-k_{CO,CO_2,c} \times\frac{M_{cat}}{V_{densebed}}\times(P_{CO})^{a_5}\times(P_{O_2})^{a_6}-k_{CO,CO_2h}\times(P)_{CO}^{a_7}\times(P_{O_2})^{a_8} \quad (25)$$

The energy balance for the dense bed including all the reactions is

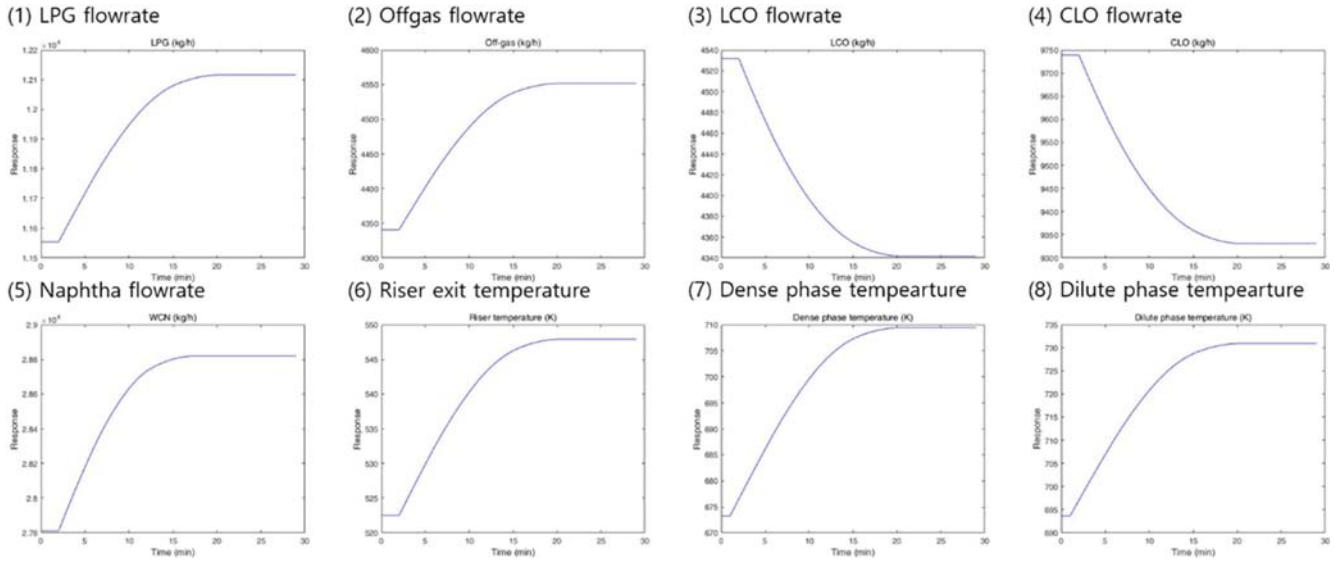

Fig. 1. Dynamic response of the FCC process to a 10% increase of the air flow rate.

$$\frac{d}{dt}((M_{cat}+M_{O_2}+M_{N_2}+M_{CO}+M_{CO_2}+M_{H_2O})\times C_{p,\,avg}\times T_{regen})$$
$$=(\dot{M}_{O_2,\,in}\times C_{p,\,O_2}\times T_{air}\times \dot{M}_{N_2,\,in}\times C_{p,\,N_2}\times T_{air}+\dot{M}_{cat}\times C_{p,\,cat}$$
$$\times T_{riser})-(\dot{M}_{O_2,\,DensetoDilute}\times C_{p,\,O_2}\times T_{regen}+\dot{M}_{N_2,\,DensetoDilute} \quad (26)$$
$$\times C_{p,\,N_2}\times T_{regen}+\dot{M}_{cat}\times C_{p,\,cat}\times T_{regen}+\dot{M}_{CO,\,DensetoDilute}$$
$$\times C_{p,\,CO}\times T_{regen}+\dot{M}_{CO_2,\,DensetoDilute}\times C_{p,\,CO_2}\times T_{regen}$$
$$+\dot{M}_{H_2O,\,DensetoDilute}\times C_{p,\,H_2O}\times T_{regen})+Q_{R,\,Densebed}V_{Densebed}$$
$$+\dot{M}_{cat}\frac{Y_{coke}^{riser}Y_{H_2}^{riser}}{MW_{H_2}}\Delta H_{H_2H_2O}$$

2-2. The Dilute Phase

The dilute phase is assumed to be pseudo steady-state since the velocity of the gaseous phase is very high. The amount of catalyst particles in the dilute phase is also very small, and thus the dilute phase can be considered as a single-phase well-mixed reactor where CO is burned homogeneously.

The material balances for CO, CO_2 and O_2 at an axial position z are given by

$$\frac{d}{dz}(\dot{M}_{CO})=-k_{CO,\,CO_2h}\times(P_{CO})^{a_7}\times(P_{O_2})^{a_8}\times A_{regen} \quad (27)$$

$$\frac{d}{dz}(\dot{M}_{CO_2})=k_{CO,\,CO_2h}\times(P_{CO})^{a_7}\times(P_{O_2})^{a_8}\times A_{regen} \quad (28)$$

$$\frac{d}{dz}(\dot{M}_{O_2})=-k_{CO,\,CO_2h}\times\frac{1}{2}\times(P_{CO})^{a_7}\times(P_{O_2})^{a_8}\times A_{regen} \quad (29)$$

3. Steady-state Simulation

The constructed FCC model was tested for various steady-state operating conditions. The main results of the riser reactor are the flow rates of products and other process variables: pressure and temperature of the reactor effluent at the riser exit. From the regenerator model, the temperature of catalyst in dilute gas phase and dense solid phase can be estimated. The result was compared to measured data from an operating FCC plant. The parameters used for simulation are given in Table 1. There were small discrepancies between the simulation results and measured data, it was observed that the simulation data points have similar trends. Because of the proprietary issue, the measured data are not shown here. However, the R^2 values for the flow rates of the product and temperature of riser exit, dense phase and dilute phase of the regenerator ranged from 0.88 to 0.98.

Table 1. Parameters of the reactor and regenerator model

Parameter	Value
Φ	0.069
μ	3.32
λ_p	0.76
μ_p	1.64
a_c	0.038
b_c	−0.054
β	0.024
a_1	0.5
a_2	0.65
a_3	0.5
a_4	0.65
a_5	0.95
a_6	0.9
a_7	0.9
a_8	0.95

4. Dynamic Simulation

Dynamic analysis of the model was performed to understand the interactions between the riser reactor and the catalyst regenerator during operation. The FCC model was tested under the step changes of the amount of air flow and catalyst circulation rate. Fig. 1 shows

the dynamic response of the model to an 10% increase of the air flow rate.

The amount of air flow determines the combustion reaction in the regenerator. When greater amount of air is supplied, more combustion reactions occur and more heat is generated. Consequently, the temperature of dense and dilute phases in the regenerator increases. A relatively hot catalyst is transferred to the riser and increases the temperature of riser reactor. The high temperature causes more cracking reactions to occur in the riser reactor. The amount of heavier products (CLO and LCO) decreased, while the amount of the lighter product (off-gas and LPG) increased.

Next, the effect of increased catalyst circulation rate by 10% was studied. When the catalyst circulation rate is increased, more energy is transferred to the riser reactor and the riser temperature is suddenly increased. As the cracking reactions are endothermic, the cracking reactions occur more often in this condition. However, as the riser and the regenerator temperature begin to decrease, the flow rate of heavier components becomes favored. The amounts of the light products increase slightly because of the increased catalyst flowrate in the riser reactor. The dynamic response of the process is shown in Fig. 2.

STRUCTURAL OBSERVABILITY ANALYSIS OF FCC PLANT SYSTEM

1. Graphical Modeling of the FCC Process

The riser reactor and the catalyst regenerator in the FCC process can be divided further into three nodes based on their functions [25]. The riser reactor consists of the feed inlet zone, reaction zone and stripping zone. The stripping zone was not modeled separately in this study because the catalyst is separated from the product rapidly and completely. However, the process state of the location should be defined for observability analysis. Meanwhile, the catalyst regenerator is divided into the dilute gas phase where the spent catalysts are fed and CO is burned, the surface between dilute phase and dense phase bed where mass and energy are transferred, and the dense solid phase where the coke on catalyst surface is burnt and the catalyst returns to the riser reactor. A directed graph consisting of these nodes is generated and shown in Fig. 3.

2. Structural Analysis

Structural analysis of the model is a way to find controllability and observability of a complex system by using a graph theory and output-set assignment method [26]. For a system associated with input-output relationships, a complex system can be analyzed to find whether the system is controllable and observable without exact state-space model [26,27].

To perform the structural analysis, all nodes, connections between the nodes, inputs and outputs of the system and measurable system variables should be identified. From input-output relationships and directed graph, a set of the modeling relationships are defined.

For the variables in the riser reactor, we have

$$f_1(x_1, x_2, x_8)=0 \quad (30)$$

$$f_2(x_2, x_3)=0 \quad (31)$$

$$f_3(x_3, x_4, x_5)=0 \quad (32)$$

The above equations explain relationships between process variables around each node in the riser reactor.

For the variables in the catalyst regenerator, we have

$$f_4(x_5, x_6, x_9, x_{11})=0 \quad (33)$$

$$f_5(x_6, x_7, x_{11})=0 \quad (34)$$

$$f_6(x_7, x_8, x_9)=0 \quad (35)$$

Eqs. (33)-(35) describe the system variables and their relationships in the catalyst regenerator.

For the whole system, we have

$$f_7(x_1, x_4, x_9, x_{10})=0 \quad (36)$$

$$f_8(x_1)=0 \quad (37)$$

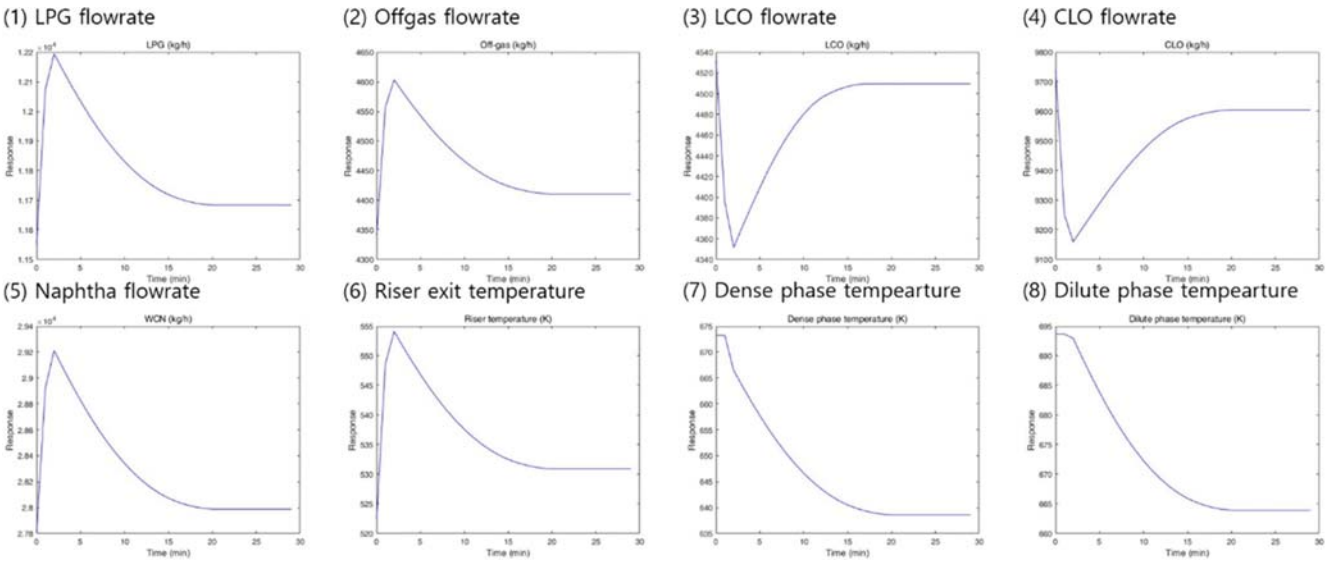

Fig. 2. Dynamic response of the FCC process to a 10% increase of catalyst circulation rate.

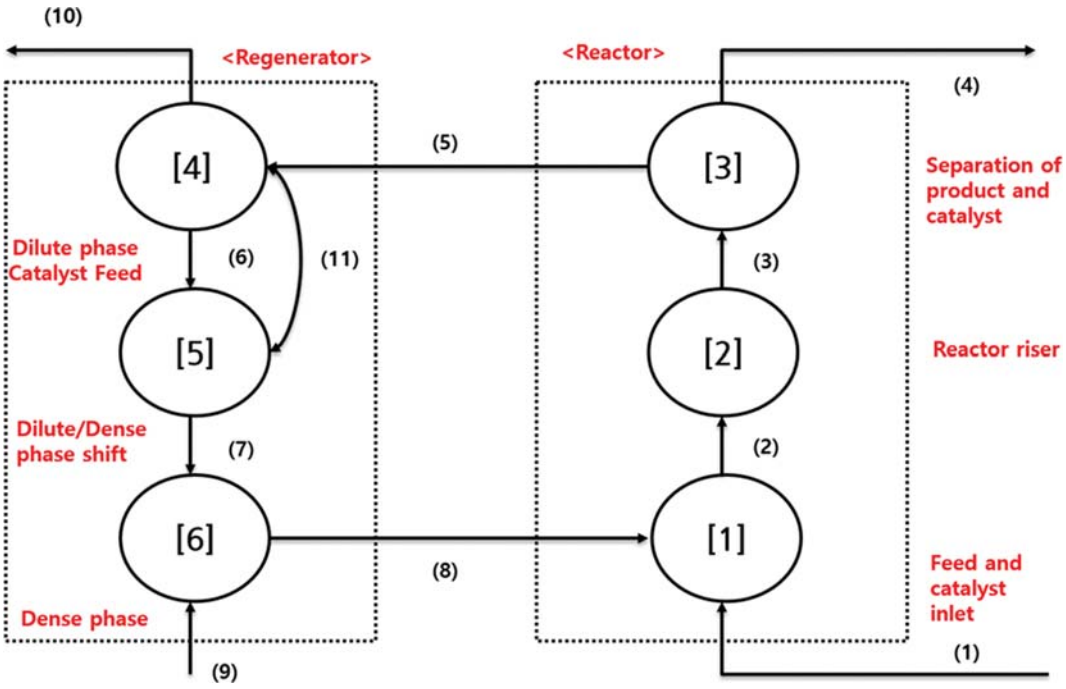

Fig. 3. A directed graph of the FCC process.

$$f_9(x_4)=0 \quad (38)$$

Eqs. (36)-(38) depict the relationships among the process feed, reactor effluent and catalyst gas outlet. The variables x_1 to x_{11} in Eqs. (30)-(38) represent the state of the edges located around each node in Fig. 3. The process variables used for the relationships are pressure, temperature and flow rates within each process that could be measured from operating FCC plant. In Eqs. (36) and (37), the compositions of feed and reactor effluent are included. For the function f_i of each node, material and energy balances proposed in Section 2 were used.

With this set of modeling relationships, no algebraic solution of the entire set was found. However, it is unnecessary to solve the system simultaneously for identification of structural observability. Instead, output-set assignment can be found by constructing an occurrence matrix from the modeling relationships and solving the subsets in the matrix sequentially [28]. This is much more effective for the structural analysis when we have a complex system whose algebraic solution is definitely unavailable or very difficult.

In the occurrence matrix, each function is placed at row and each state variable is placed in the column. Assignments are marked as X in the corresponding position in the matrix of Fig. 4.

Output-set assignment algorithm begins at a position in the occurrence matrix where the equation can be solved spontaneously. It must be a complete submodel with any node or edges where all the measurements are available. In this study, only the first node and edge have the complete data for its submodel, making them as the starting point of the algorithm. Then, every function in which

	x1	x2	x3	x4	x5	x6	x7	x8	x9	x10	x11
F1	x	x						x			
F2		x	x								
F3			x	x	x						
F4					x	x					x
F5						x	x				x
F6							x	x		x	
F7	x				x				x	x	
F8	x										
f9				x							

Fig. 4. Occurrence matrix of the relationship set.

variables of the solved system are included is analyzed to find another function which becomes solvable with the result from the previous step. The algorithm is repeated until every function is assigned to system variables. However, we found that not every function was solvable with given modeling relationships.

Functions and system variables which found assignment are gathered in the form of a diagonal matrix. Gathered output-set is the complete output set which can be controlled and observed. The rest of the functions and system variables are called incomplete output-set and are not controllable or observable. Fig. 5 shows the complete output-sets and incomplete sets.

This result gives answer to the question whether each node of graph model is observable. If any node, location or process state variable of the system is in the complete output set, then systematically observable. However, if it is in the incomplete output set, then the state is unobservable. In our system, five system variables and three nodes are identified to be observable and controllable. Three nodes in the reactor including feed inlet zone, riser reactor and separation zone are completely observable. In addition, the edges in the reactor are completely observable. However, in the regenerator, most of the edges were not controllable. This is because of the lack of measurements in the regenerator.

3. Completing the Assignment for Finding Optimal Place for Additional Measurements

The previous section found that the FCC system is not perfectly observable due to the lack of measurements. To complete the assignment, it was assumed that additional system variable which was unassigned became available by additional measurements. In our occurrence model two variables among x_6 to x_{11} are considered as the known variables for each case study. By this assumption, the assignment algorithm can be continued at any unmeasured variable.

By completing the assignment as explained in Fig. 6, the optimal location of additional measurement is suggested. We found that gas effluent and regenerated catalyst which is recycled to the

	x1	x4	x2	x3	x5	x6	x7	x8	x9	x10	x11
F8	X(1)										
F9		X(2)									
F1	x		X(3)					X			
F2			x	X(4)							
F3		X		x	X(5)						
F4					x	x			x		x
F5						x	x				x
F6							x	x	x		
F7	x	x							x	x	

5x5 Complete output-set : Observable Incomplete output-set : Unobservable

Fig. 5. Occurrence matrix with complete output-set analysis.

	x1	x4	x2	x3	x5	x6	x7	x8	x9	x10	x11
F8	X(1)										
F9		X(2)									
F1	x		X(3)					X			
F2			x	X(4)							
F3		X		x	X(5)						
F4					x	x(8)			x		x
F5						x(9)	x				x
F6							x(7)	x(*)	x		
F7	x	x							x(6)	x(*)	

5x5 Complete output-set : Observable Complete output-set : Observable!
(4x4 w/ more measurement)

Fig. 6. Completing the occurrence matrix with complete output-set analysis.

feed inlet zone in the reactor is the most optimal location for additional measurements, meaning that adding a minimal number of sensors can achieve full observation of the system. Assigning the entire system with a single additional measured variable was infeasible in this modeling relationship.

CONCLUSION

Using the discrete lumped group method, the FCC process was investigated to develop a process model for a fluid catalytic cracker unit. This model predicts the product yield and other process states under steady-state and dynamic conditions. A yield function for the kinetic model of the riser was constructed and applied to the model. Using this model, steady-state simulation results and dynamic responses to change of process variables were presented. In addition, structural analysis of the fluid catalytic cracking process was performed to investigate observability of the FCC system. A directed graph was drawn to construct modeling relationships of the system. The reactor and regenerator unit in this system were divided into six nodes based on their functions. The modeling relationships were built based on the nodes and edges of the directed graph. Output-set assignment algorithm was demonstrated on the occurrence matrix which is made of modeling relationships. The suggested approach can help in performing model-based optimization and control of the FCC process and other complex processes in a systematic manner.

ACKNOWLEDGEMENT

This research was supported by the Korea Ministry of Trade, Industry and Energy as "Development of Conceptual Framework for Knowledge-based Plant O&M (10082580)." This research was respectfully supported by Engineering Development Research Center (EDRC) funded by the Ministry of Trade, Industry & Energy (MOTIE) (No. N0000990).

NOMENCLATURE

ε : void fraction
ρ_{cat} : bulk catalyst density [kg/m^3]
ρ_g : gas density [kg/m^3]
θ : temperature cut point [K]
Φ : catalyst activity coefficient
ϕ : coking tendency
A_i : pre-exponential factor of i^{th} pseudo-component [kJ/mol]
A_{riser} : cross-sectional area of the riser [m^2]
A_{regen} : cross-sectional area of the regenerator [m^2]
BP_i : boiling point of the i^{th} pseudo-component [K]
$\dot{C}$: coke mass flow rate [kg/h]
$\dot{C}_0$: coke flow rate at the riser inlet zone [kg/h]
C_D : drag coefficient
$E_{A,i}$: activation energy of the i^{th} pseudo-component [kJ/mol]
$H_{c,coke}$: heat of combustion of coke [kJ/kg]
$H_{c,i}$: heat of combustion of i^{th} pseudo-component [kJ/kg]
ΔH_i : heat of cracking of i^{th} pseudo-component [kJ/kg]
$\Delta H_{C,CO}$: heat of combustion in reaction I [kJ/mol]
$\Delta H_{C,CO_2}$: heat of combustion in reaction II [kJ/mol]
$\Delta H_{CO,CO_2}$: heat of combustion in reaction III and IV [kJ/mol]
$\Delta H_{H_2,H_2O}$: heat of combustion in reaction V [kJ/mol]
$\Delta H_{vap,i}$: heat of vaporization of i^{th} pseudo-component [kJ/kg]
$\dot{M}_{CO}$: molar flow rate of CO [mol/h]
$\dot{M}_{CO_2}$: molar flow rate of CO_2 [mol/h]
$\dot{M}_{O_2}$: molar flow rate of O_2 [mol/h]
$\dot{M}_{N_2}$: molar flow rate of N_2 [mol/h]
$\dot{M}_{HVGO}$: molar flow rate of the feed [mol/h]
$\dot{M}_{H_2O}$: molar flow rate of H_2O [mol/h]
$\dot{M}_{CO,\,DensetoDilute}$: molar flow rate of CO leaving the dense bed [mol/h]
$\dot{M}_{CO_2,\,DensetoDilute}$: molar flow rate of CO_2 leaving the dense bed [mol/h]
$\dot{M}_{N_2,\,AirtoDense}$: molar flow rate of N_2 from air to the dense bed [mol/h]
$\dot{M}_{H_2O,\,DensetoDilute}$: molar flow rate of H_2O leaving the dense bed [mol/h]
$\dot{M}_{O_2,\,DensetoDilute}$: molar flow rate of O_2 leaving the dense bed [mol/h]
$\dot{M}_{O_2,\,in}$: molar flow rate of O_2 from the air to the dense bed [mol/h]
M_{cat} : total catalyst holdup in the dense bed [kg]
$\dot{M}_i$: mass flow rate of ith pseudo-component [kg/h]
$\dot{M}$: mass flow rate of pseudo-components [kg/h]
$\dot{M}_{cat}$: mass flow rate of catalyst [kg/h]
$\dot{M}_{steam}$: mass flow rate of steam [kg/h]
MW : average molecular weight [kg/mol]
MW_i : molecular weight of i^{th} pseudo-component [kg/mol]
MW_{coke} : molecular weight of coke [kg/kmol]
MW_{H_2} : molecular weight of hydrogen [kg/kmol]
N : number of pseudo-components
NBP : normal boiling point [K]
P : pressure [atm]
P_{CO} : partial pressure of CO [atm]
P_{O_2} : partial pressure of O_2 [atm]
$Q_{R,\,Densebed}$: heat released per volume due to combustion reactions in the dense bed [kJ/m^3]
$Q_{R,\,Dilutebed}$: heat released per volume due to combustion reactions in the dilute phase [kJ/m^3]
R : ideal gas constant
$T_{B,i}$: boiling point temperature of i^{th} pseudo-component [K]
T : temperature [K]
$v_{T_{Dilute}}$: temperature of dilute phase [K]
$T_{mixzone}$: temperature of feed inlet zone [K]
T_{HVGO} : temperature of liquid feed [K]
T_{regen} : temperature of the dense phase regenerator [K]
T_{steam} : steam temperature [K]
$V_{Densebed}$: volume of the dense bed [m^3]
Y_{cokr}^{Riser} : coke weight fraction on catalyst from the riser reactor to regenerator
Y_{coke}^{Regen} : coke weight fraction on catalyst from the regenerator to riser reactor
Y_{coke} : coke weight fraction on catalyst
$Y_{H_2}^{Coke}$: H_2 weight fraction in coke
C_{p,O_2} : heat capacity of oxygen [kJ/(mol K)]

C_{p,N_2} : heat capacity of nitrogen [kJ/(mol K)]
$C_{p,CO}$: heat capacity of CO [kJ/(mol K)]
C_{p,CO_2} : heat capacity of CO_2 [kJ/(mol K)]
C_{p,H_2O} : heat capacity of H_2O [kJ/(mol K)]
$C_{p,cat}$: heat capacity of catalyst [kJ/(mol K)]
$C_{p,avg}$: average heat capacity [kJ/(mol K)]
$C_{p,gas,i}$: heat capacity of the i^{th} pseudo-component in gas phase [kJ/(mol K)]
$C_{p,liquid,i}$: heat capacity of the i^{th} pseudo-component in liquid phase [kJ/(mol K)]
$C_{p,steam}$: steam heat capacity [kJ/(mol K)]
d_{cat} : catalyst particle diameter [m]
g : gravitational acceleration [m/s^2]
k_i : cracking rate constant of the i^{th} pseudo-component [mol/(m^3 h)]
$k_{C,CO}$: reaction rate constant in reaction I [1/(atm h)]
k_{C,CO_2} : reaction rate constant in reaction II [1/(atm h)]
$k_{CO,CO_2,c}$: reaction rate constant in reaction III [mol/(kgcat h atm^2)]
$k_{CO,CO_2,h}$: reaction rate constant in reaction IV [mol/(h atm^2)]
p(i, j) : yield function of a reaction where the component i is converted to j
$r_{C,CO}$: rate of reaction I [mol/(m^3 h)]
r_{C,CO_2} : rate of reaction II [mol/(m^3 h)]
$r_{C,CO_2,c}$: rate of reaction III [mol/(m^3 h)]
$r_{C,CO_2,h}$: rate of reaction IV [mol/(m^3 h)]
v_{cat} : velocity of the catalyst in riser reactor [m/h]
v_g : gas velocity in riser reactor [m/h]
w_i : weight fraction of the i^{th} pseudo-component
z : axial position [m]

REFERENCES

1. R. Sadeghbeigi, Fluid Catalytic Cracking Handbook: Design, Operation, and Troubleshooting of FCC facilities, Elsevier (2000).
2. R. J. Quann and S. B. Jae, *Ind. Eng. Chem. Res.*, **31**(11), 2483 (1992).
3. R. K. Gupta, V. Kumar and V. K. Srivastava, *Chem. Eng. Sci.*, **62**(17), 4510 (2007).
4. V. W. Weekman, Lumps, Models and Kinetics in Practice, American Institute of Chemical Engineers (2000).
5. V. W. Weekman Jr. and D. M. Nace, *AIChE J.*, **16**(3), 397 (1970).
6. L.-S. Lee, Y. W. Chen, T. N. Huang and W. Y. Pan, *Can. J. Chem. Eng.*, **67**(4), 615 (2007).
7. I. S. Han and C. B. Chung, *Chem. Eng. Sci.*, **56**(5), 1951 (2001).
8. C. Jia, S. Rohani and A. Jutan, *Chem. Eng. Process.: Process Intensification*, **42**(4), 311 (2003).
9. R. Roman, Z. K. Nagy, M. V. Cristea and S. P. Agachi, *Comput. Chem. Eng.*, **33**(3), 605 (2009).
10. G. M. Bollas, A. A. Lappas, D. K. Iatridis and I. A. Vasalos, *Catal. Today*, **127**, 31 (2007).
11. J. Corella abd E. Frances, *Stud. Surf. Sci. Catal.*, **68**, 375 (1991).
12. S. M. Jacob, B. Gross, S. E. Voltz and V. W. Weekman, *AIChE J.*, **22**(4), 701 (1976).
13. A. Arbel, Z. Huang, I. H. Rinard, R. Shinnar and A. V. Sapre, *Ind. Eng. Chem. Res.*, **34**(4), 1228 (1995).
14. S. Kumar, A. Chadha, R. Gupta and R. Sharma, *Ind. Eng. Chem. Res.*, **34**(11), 3737 (1995).
15. Y. Y. Liu, J. J. Slotine and A. L. Barabasi, *Proc. National Academy of Sci.*, **110**(7), 2460 (2012).
16. K. J. Reinschke, Multivariable Control: A Graph Theoretic Approach, Springer-Verlag (1988).
17. M. Anushka, S. Perera, B. Lie and C. Fernando, *Modeling, Identification and Control*, **36**(3), 189 (2015).
18. J. L. Fernandes, J. J. Verstraete, C. I. Pinheiro, N. M. C. Oliveira and F. R. Ribeiro, *Chem. Eng. Sci.*, **62**(4), 1184 (2007).
19. T. S. Pugsley and F. Berruti, *Powder Technol.*, **89**(10), 57 (1996).
20. Y. S. Won, A. Jeong, J. Choi, S. Jo, H. Ryu and C. Yi, *Korean J. Chem. Eng.*, **34**(3), 913 (2017).
21. R. V. Shendye and R. A. Rajadhyaksha, *Chem. Eng. Sci.*, **47**(3), 661 (1992).
22. D. M. Nace, *Ind. Eng. Chem. Prod. Res. Dev.*, **8**(1), 24 (1969).
23. M.-R. Riazi, Characterization and Properties of Petroleum Fractions, ASTM International (2005).
24. Y. S. Won, D. Kim and J. Choi, *Korean J. Chem. Eng.*, **35**(3), 812 (2018).
25. J. L. Fernandes, C. I. C. Pinheiro, N. M. C. Oliveria, A. I. Neto and F. R. Ribeiro, *Chem. Eng. Sci.*, **62**(22), 6308 (2007).
26. J. A. Bondy and U. S. R. Murty, Graph Theory with Applications, Elsevier (1982).
27. I. Ponzoni, M. C. Sanchez and N. B. Brignole, *Ind. Eng. Chem. Res.*, **38**, 3027 (1999).
28. I. Ponzoni, M. C. Sanchez and N. B. Brignole, *Ind. Eng. Chem. Res.*, **43**, 577 (2004).